



# On the run-out distance of geophysical gravitational flows: Insight from fluidized granular collapse experiments

O. Roche <sup>a,b,c,\*</sup>, M. Attali <sup>a,b,c</sup>, A. Mangeney <sup>d</sup>, A. Lucas <sup>e</sup>

<sup>a</sup> Clermont Université, Université Blaise Pascal, Laboratoire Magmas et Volcans, BP 10448, F-63000 Clermont-Ferrand, France

<sup>b</sup> CNRS, UMR 6524, LMV, F-63038 Clermont-Ferrand, France

<sup>c</sup> IRD, R 163, LMV, F-63038 Clermont-Ferrand, France

<sup>d</sup> Institut de Physique du Globe de Paris, Equipe Sismologie, CNRS-UMR 7154, Université Paris Diderot 7, PRES Sorbonne Paris Cité, Paris, France

<sup>e</sup> California Institute of Technology, Division of Geological and Planetary Sciences, Pasadena, CA, USA

## ARTICLE INFO

### Article history:

Received 10 February 2011

Received in revised form 12 September 2011

Accepted 14 September 2011

Available online xxx

Editor: Y. Ricard

### Keywords:

granular flow  
rock avalanche  
Valles Marineris landslides  
pyroclastic flow  
run-out  
experimental scaling law

## ABSTRACT

We present the results of laboratory experiments on the emplacement of gravitational granular flows generated from axisymmetrical release of columns of fine ( $\sim 75 \mu\text{m}$ ) or coarse ( $\sim 330 \mu\text{m}$ ) particles initially fluidized with air. Internal friction is first negligible in the granular columns and then increases as pore pressure diffuses within the propagating flows, which are thus characterized by a mean friction lower than that of dry (i.e., non fluidized) flows. For columns of height-to-radius ratios  $a \approx 0.2\text{--}30$ , we identify the modes of flow propagation and the scaling laws that characterize the morphology of the resulting deposits. Here we show that the normalized run-out distance of the initially fluidized flows scales as a power law of  $a$  (i.e.,  $\lambda a^n$ ), thus demonstrating that this scaling law is not only typical of dry granular flows, as claimed in the literature. Fluidization reduces contacts between the grains and thus effective energy dissipation. Its effect increases the coefficient  $\lambda$  compared to dry flows but it has no influence on the exponent  $n$  that decreases from 1 to 1/2 at increasing  $a$ , mainly due to axisymmetrical spreading as shown by earlier works on dry coarse particles, except for the initially dry flows of fine particles at  $a > \sim 2$  as it decreases to  $\sim 2/3$ . In this latter case the flows could experience (partial) auto fluidization as their normalized flow run-out is equal to that of their initially fluidized counterparts at  $a > \sim 4$ . The auto fluidization mechanism, supported by other recent experimental works, is particularly appealing to account for the long run-out distance of natural dense gas-particle mixtures such as pyroclastic flows. At high  $a$ , fluidization also affects the generation of surface waves with clear signatures on the deposits. We compare our experimental results with published data on Valles Marineris landslides (Mars) whose emplacement mechanisms are controversial. These natural events are characterized by values of  $\lambda$  higher than that of the laboratory flows, including those with low friction. This shows that some mechanism and/or scale effects promoted energy dissipation for the VM landslides that was significantly smaller than for typical dry frictional granular materials, as suggested by Lucas and Mangeney (2007).

© 2011 Elsevier B.V. All rights reserved.

## 1. Introduction

Gravity driven granular flows are common events at the surfaces of the Earth and of other planets. They consist of solid particles commonly mixed with an interstitial lighter fluid (liquid or gas) that may interact with the grains and decrease the intensity of their contacts, thus reducing energy dissipation and favoring propagation. Examples include subaerial or subaqueous rock avalanches (i.e., landslides), snow avalanches, debris flows, and volcanic phenomena such as

pyroclastic flows and debris avalanches. Their volumes are up to  $\sim 10^{11} \text{m}^3$  in terrestrial subaerial environments and up to  $\sim 10^{13} \text{m}^3$  for submarine and extraterrestrial events (see references in Legros, 2002). These granular flows can travel distances up to several kilometers, so that subaerial flows on Earth represent important natural hazards. As discussed extensively in literature, long flow run-out distance can have various causes, including a lubrication layer generated by an air cushion (Shreve, 1968) or basal melting (De Blasio and Elverhøi, 2008; Goren and Aharonov, 2007), fluidization by a fluid of internal or external source (Hung and Evans, 2004), acoustic fluidization (Collins and Melosh, 2003), destabilization of a loose granular substrate (Iverson et al., 2011; Mangeney, 2011; Mangeney et al., 2007, 2010), or friction reduction caused by segregation effects (Linares-Guerrero et al., 2007; Phillips et al., 2006; Roche et al., 2005). Predicting the run-out distance of geophysical granular flows is crucial for hazards assessment and requires identifying the control parameters, which represents a challenging issue.

\* Corresponding author at: Clermont Université, Université Blaise Pascal, Laboratoire Magmas et Volcans, BP 10448, F-63000 Clermont-Ferrand, France. Tel.: +33 4 73346768; fax: +33 4 73346744.

E-mail addresses: [o.roche@opgc.univ-bpclermont.fr](mailto:o.roche@opgc.univ-bpclermont.fr) (O. Roche), [m.attali@opgc.univ-bpclermont.fr](mailto:m.attali@opgc.univ-bpclermont.fr) (M. Attali), [mangeney@ipgp.fr](mailto:mangeney@ipgp.fr) (A. Mangeney), [alucas@caltech.edu](mailto:alucas@caltech.edu) (A. Lucas).

Several methods are proposed in literature to describe quantitatively the run-out distance of gravitational granular flows and to assess the degree of energy dissipation. The ratio of the run-out distance over the vertical fall height, known as the Heim coefficient, has been long assumed to represent the inverse of a mean effective friction coefficient (i.e., representative of the mean energy dissipation during the flow if a simple Coulomb frictional behavior is assumed). This ratio, however, increases with the volume of the deposit (e.g., Hayashi and Self, 1992; Legros, 2002; McEwen, 1989), as confirmed by analytical and numerical modeling of granular collapse (see Eq. (5) of Lucas and Mangeney, 2007; Staron, 2008; Staron and Lajeunesse, 2009), and hence is not appropriate to describe the mean effective friction. Instead, Lucas and Mangeney (2007) propose to use the ratio of the run-out distance over the initial thickness of the released mass, which eliminates the artificial volume dependence and therefore reflects more accurately the inverse of the mean energy dissipation during the flow. The high values of this ratio (typically  $\sim 10$ ) that characterize many large natural landslides suggest an effective friction significantly smaller than what would be expected from purely dry granular flows, as confirmed by back analyses of natural landslides (e.g., Kuo et al., 2009; Lucas and Mangeney, 2007; Pirulli and Mangeney, 2008).

Recent experimental works on flows generated from dry granular column collapse offer a straightforward and powerful way to quantify, under controlled conditions, the run-out as a function of the geometrical characteristics of the mobilized granular mass. They reveal that the flows have a run-out distance that obey a well-defined unique scaling law independently of the volume of the material and primarily depends on the height-to-radius ratio of the columns (e.g., Balmforth and Kerswell, 2005; Lajeunesse et al., 2004; Lube et al., 2004). Analytical and numerical simulations of these experiments, typically at ratios  $\sim 1$ , allow relating the parameters involved in the scaling laws to the frictional properties of the granular media and to the experimental configuration (channel or axisymmetrical collapse) (e.g., Kerswell, 2005; Mangeney-Castelnau et al., 2005; Staron and Hinch, 2005; Zenit, 2005). One of the key questions in prospect of using these scaling laws for interpretation of natural events is as to whether they are a typical signature of dry granular flow processes, as claimed in the literature (e.g., Lajeunesse et al., 2006; Staron, 2008), or if they could also characterize flows with much less energy dissipation.

In order to address this issue, we carried out new experiments on axisymmetrical granular column collapse. In this paper, we investigate the scaling laws of the run-out distance of flows generated from fluidized columns and whose mean effective friction during emplacement is significantly smaller than that of typical dry granular materials. The geometrical configuration applies well to large-scale granular flows generated, for instance, from cliff collapse and that propagate over a rather flat and laterally unconfined topography. We stress that low effective friction is obtained through initial fluidization but could be achieved in nature by other means as mentioned above (e.g., lubrication layer, acoustic fluidization, substrate destabilization, segregation effects). After analysis of the experimental flow dynamics and deposits, experimental results are compared with natural data of some Martian landslides whose emplacement mechanisms are controversial. Then, we follow the method of Lucas and Mangeney (2007) to discuss the dynamics of these landslides (for which the original height-to-radius ratio is  $< 1$ ) in terms of effective friction in the context of thin layer (i.e., depth-averaged) models.

## 2. Scaling laws of dry granular column collapse

### 2.1. Earlier experimental studies

The experimental investigations of Lajeunesse et al. (2004) and Lube et al. (2004), involving dry and relatively coarse particles of typical grain size of a few hundreds of microns to a few millimeters, show that the deposit characteristics of flows generated from column collapse on a

horizontal plane in the axisymmetrical configuration (hereafter called 3D for convenience) are controlled primarily by the column aspect ratio

$$a = \frac{h_i}{r_i}, \quad (1)$$

where  $h_i$  and  $r_i$  are the height and radius of the column, respectively (Fig. 1). Three deposit morphologies are identified at increasing  $a$ , that is, truncated-cone generated by flank avalanches, and cone or cone with a bulge (“Mexican-hat” of Lajeunesse et al., 2004) as the whole column collapses (Fig. 1). These works reveal scaling laws that characterize the geometrical parameters of the deposits for  $a \sim 0.5\text{--}30$ . The final deposit length,  $r_f$ , and height,  $h_f$ , (see Fig. 1) are used to define the normalized run-out distance

$$r^* = \frac{r_f - r_i}{r_i}, \quad (2)$$

and the normalized deposit height

$$h^* = \frac{h_f}{r_i}, \quad (3)$$

which helps to identify scaling laws of the form

$$r^*, h^* = \lambda a^n, \quad (4)$$

where the coefficient  $\lambda$  and the exponent  $n$  are determined by fitting the experimental data (Table S1, supplementary material). As mentioned by the authors,  $r_f - r_i$  and  $h_f$  could be normalized by  $h_i$  instead of  $r_i$ , and we note that in that case  $r^*, h^* = \lambda a^{n-1}$ . A notable result concerning  $r^*$  is that  $n = 1$  at  $a < 1.5\text{--}3$  whereas  $n = 1/2$  at  $a > 1.5\text{--}3$ . This transition may reflect influence of the axisymmetrical spreading of the granular mass at increasing  $a$  as shown by Lajeunesse et al. (2004) from a heuristic model. This is supported by experiments on flows in channels (hereafter called 2D for convenience, see Table S1) for which material spreading is unidirectional. From the compilation we present in Table S1, we note that at high  $a$ , the exponent  $n$  is different in the various studies but it approaches one as the channel width increases so that side effects become less important (Balmforth and Kerswell, 2005; Lacaze et al., 2008; Lajeunesse et al., 2005; Lube et al., 2005; Mériaux, 2006). The study of Lube et al. (2004) suggests that these scaling laws are not influenced by the particle shape (spherical, angular) or the nature of the substrate (smooth, rough, erodible). In contrast, the 2D experiments of Balmforth and Kerswell (2005) show that the coefficient  $\lambda$  is dependent on the type of granular material. Concerning the normalized height in 3D experiments,  $h^* = a$  (that is  $h_f = h_i$ ) at low aspect ratios as the deposits are truncated cones, whereas at higher aspect ratios  $h^*$  is either constant (Lajeunesse et al., 2004) or shows a weak variation with  $a$  (Lube et al., 2004; Table S1). Other experimental works in 2D explore the influence of the interstitial fluid phase and/or of the polydispersity of the granular material (Girolami et al., 2008, 2010; Meruane et al., 2010; Phillips et al., 2006; Roche et al., 2002, 2005, 2008; Thompson and Huppert, 2007). However, they consider a limited range of column aspect ratio ( $a \sim 1\text{--}3$ ) and do not offer the opportunity to identify scaling laws as described above.

### 2.2. Insights from analytical and numerical studies

Discrete and continuum simulations at low  $a$  reproduce quantitatively the values of the exponent  $n$  of the experimental scaling laws (e.g., Kerswell, 2005; Mangeney-Castelnau et al., 2005; Staron and Hinch, 2005; Zenit, 2005). Discrete element models, however, reveal contrasting results as some of them significantly overestimate the run-out distance compared to laboratory experiments (i.e., higher  $\lambda$  values) when considering an intergranular friction coefficient typical of the experimental material (Staron and Hinch, 2005; Zenit, 2005)

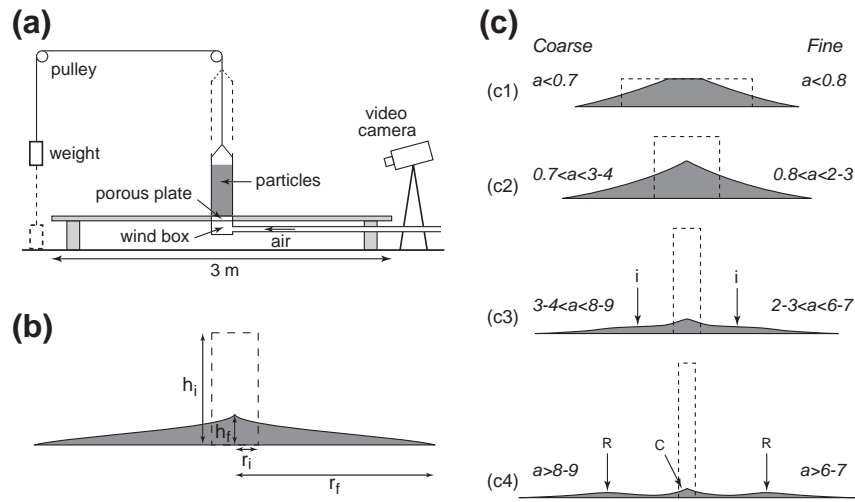


**Fig. 1.** Experimental device and deposit morphologies. (a) Apparatus. (b) Geometrical parameters of the initial granular column (dashed line) and of the final deposit (gray). (c) Deposit shapes at increasing  $a = h_i/r_i$ . Cases (c1–3) were identified in earlier studies involving dry coarse particles. Corresponding values of  $a$  in our study are shown for the coarse and fine particles in case of dry columns. (c1) Truncated cone, (c2) cone, (c3) “Mexican-hat” characterized by an inflection point ( $i$ ) so that the deposit surface is concave-upward and then convex-upward downstream (Lajeunesse et al., 2004), and (c4) cone-and-ridge where (C) and (R) denote the central cone and the circular ridge, respectively. In (c4), the deposits exhibit up to three distinct ridges. In all cases, the central area above the porous plate is horizontal when the granular column is fluidized.

while others successfully simulate experimental data (Lacaze et al., 2008). On the other hand, thin layer depth averaged models reproduce quantitatively the experimental run-out using an effective friction angle of  $\sim 30^\circ$  (Kerwell, 2005; Mangeney-Castelnau et al., 2005), just a few degrees higher than the friction angle of the material involved. Higher friction coefficients have to be used because this approach overestimates driving forces related to pressure gradients (Mangeney et al., 2006). Analytical solutions of the thin layer equations by Lucas and Mangeney (2007), based on the works of Mangeney et al. (2000) and Kerwell (2005), predict that  $n$  is independent of the material properties and of the slope of the topography while  $\lambda$  is inversely proportional to the difference between the tangent of the effective friction angle ( $\delta$ ) and the tangent of the bed slope angle ( $\theta$ ) so that

$$r^* = \frac{\alpha a}{\tan \delta - \tan \theta}, \quad (5)$$

where  $\alpha$  is a constant and, according to Eq. (4),  $\lambda = \alpha/(\tan \delta - \tan \theta)$ . Note that Eq. (5) results from thin layer equations that are strictly valid for small  $a$  ( $< 1$ ) and dry granular flows with constant friction angle (Mangeney et al., 2010; Mangeney-Castelnau et al., 2005), so its applicability at large  $a$  and to fluidized flows is an open question. Furthermore, no experimental validation of Eq. (5) for materials with different friction angles has been provided yet. Here we investigate this issue by considering both fluidized and dry flows characterized by different mean effective friction (i.e.,  $\delta$ ) and by small to high initial aspect ratios. We use Eq. (5) as an empirical relation in order to estimate the mean effective friction over the flow duration, even though the real friction coefficient may vary with flow properties (Pouliquen and Forterre, 2002) or with time (as in initially fluidized flows).

### 3. Experimental procedure and dimensional issues

Our experimental apparatus consists of a vertical perspex cylinder that contains the granular material before release, located at the center of a horizontal smooth wooden plane of size  $3 \times 3 \text{ m}^2$  (Fig. 1). The cylinder has a radius  $r_i = 2.1\text{--}4.6 \text{ cm}$  and  $h_i$  varies from 1.1 to 64.5 cm, so that  $a$  is in the range 0.24–30.7. The cylinder is lifted rapidly, during 5–10% of the flow duration, so that spreading of the granular column is negligible while the cylinder is completely removed. This is done by means of a counterweight, thus ensuring release at consistent speed, and the granular material then spreads radially on the plane until it comes to halt.

Moisture effects are reduced as much as possible as the particles are dried in a fluidization rig and then transferred rapidly into the cylinder. The final deposit is characterized by a run-out distance,  $r_f$ , and a central height,  $h_f$ . The distance  $r_f$  is measured along eight lines, drawn from the center of the plane at  $45^\circ$  to each other, in order to determine a mean flow run-out. Experiments are recorded with a high speed video camera at 50–100 frame/s to allow for analysis of the column collapse processes and of the flow kinematics.

The study deals with the spreading of both dry and initially fluidized granular columns. In the latter case, air is injected into a wind box and then passes through a porous plate of mean pore size of  $20 \mu\text{m}$  and on which the granular material rests. The air flow rate is controlled by a flow meter at 1 bar ( $10^5 \text{ Pa}$ ) and does not vary while the column is collapsing as pressure changes of a few thousands of Pa (estimated from  $h_i$ ) are negligible compared to the ambient pressure. The granular material in the cylinder is fluidized when the air velocity, equivalent to the mean volumetric flow rate divided by the cross sectional area of the cylinder, is equal to the minimum fluidization velocity  $U_{mf}$  (Table S2, supplementary material), as classically defined for gas-fluidized systems (Geldart, 1986). At that stage, the drag generated by the upward interstitial air flow counterbalances the weight of the particles, thus promoting associated high interstitial air pore pressure and negligible intergranular friction. Note that, though fluidized, the granular column is not expanded. Once the column is released, the subsequent flow defluidizes while the pore pressure diffuses as no air is provided from the horizontal plane, and in consequence internal friction increases. The flow, however, has a mean friction (i.e., averaged on the flow duration) lower than that of a dry (i.e., initially non fluidized) equivalent. The air flux passes through the porous plate during the column collapse and is turned off after the flow has stopped.

The particles are “fine” ( $d \sim 75 \mu\text{m}$ ) and “coarse” ( $d \sim 330 \mu\text{m}$ ) well sorted glass beads whose characteristics are presented in Table S2. The flow dynamics depends on the pore pressure number,  $Pr = t_f/t_d$  (Iverson and Denlinger, 2001), where  $t_f$  is the characteristic flow duration and  $t_d = h^2/D$  is the pore pressure diffusion timescale, with  $h$  the typical flow height, and  $D$  the diffusion coefficient (values from Montserrat et al., 2007). Note that we choose  $t_f = r_f/(gh_i)^{1/2}$  (in contrast to Iverson and Denlinger, 2001, who consider  $t_f = (r_f/g)^{1/2}$ ), based on Eqs. (4) and (5) of Mangeney et al. (2010), where  $g$  is the gravitational acceleration. For typical values  $h_i = 10\text{--}50 \text{ cm}$ ,  $r_f = 10\text{--}40 \text{ cm}$ , and  $h = 0.5\text{--}1.5 \text{ cm}$ ,  $Pr$  for the coarse particles ( $Pr \sim O(10^2)$ ) is high and two orders of magnitude larger than for the fine ones ( $Pr \sim O(1)$ ).

These values of  $Pr$  indicate that pore pressure diffusion is fast compared to the flow duration for the coarse particles, and in consequence intergranular friction is reacquired very rapidly. In contrast, the pore pressure diffusion timescale is similar to the duration of the flows of fines, which have negligible internal friction for most their propagation (Roche et al., 2008, 2010). This leads to two distinct flow behaviors, as described hereafter.

## 4. Results

### 4.1. Flow and deposit characteristics

#### 4.1.1. Experiments with coarse particles

Experiments involving the dry coarse particles reproduce the results of previous studies described in Section 2.1. They reveal, however, that a wave forms at the flow surface at  $a > \sim 7$ –8 (Fig. 2). This wave travels downstream and overtakes the flow front, thus leading to a brief acceleration just before the front stops abruptly (Fig. 3). This late acceleration follows the three emplacement phases typical of flows at lower  $a$  (i.e., acceleration, constant velocity, and deceleration; Lajeunesse et al., 2004; Lube et al., 2004). The amplitude of the wave grows as the top of the column falls vertically, is maximum just after the column height has decreased to about that of the flow, and then decreases. The wave forms after the cylinder is completely removed, but its initiation due to disturbance caused by lifting cannot be excluded. Our experiments reveal a new deposit morphology at high  $a$ , in addition to those reported in earlier studies (Fig. 1). It appears at  $a > 8$ –9, thus suggesting

a link with the formation of the wave. This morphology resembles a pronounced “Mexican-hat” but its surface slope is locally positive downstream as it consists of a depression delimited by a central cone and a circular ridge located approximately half way between the front of the deposit and the cone. Therefore, it is referred to “cone-and-ridge” deposit hereafter.

Initial fluidization of the columns of coarse particles has little influence on the collapse processes. The central part of the deposits, however, is horizontal above the porous plate where the material is continuously fluidized. The flow kinematics are almost the same as that of the initially dry cases. At high  $a$ , however, the front accelerates right after release more strongly than for the dry flows (Fig. 3). It subsequently propagates at nearly constant speed, and then slightly accelerates and finally decelerates abruptly before it stops. Note that initial fluidization slightly increases the flow run-out, as discussed hereafter.

#### 4.1.2. Experiments with fine particles

Experiments with initially dry fine particles also reveal a traveling wave at the flow surface. Compared to the coarse particles, it appears at smaller aspect ratios  $a \sim 4$ –5 and leads to the formation of a ridge at  $a \sim 6$ –7 (Fig. 4a). A major difference with the coarse particles is that up to 4–5 successive shock waves form as  $a$  increases, at increasing distance from the initial column (Fig. 4b). These waves result in a non uniform flow front propagation with transient acceleration and deceleration phases, particularly at high  $a$  (Fig. 3b). They form at nearly constant rate once the flow front decelerates while the material behind it propagates

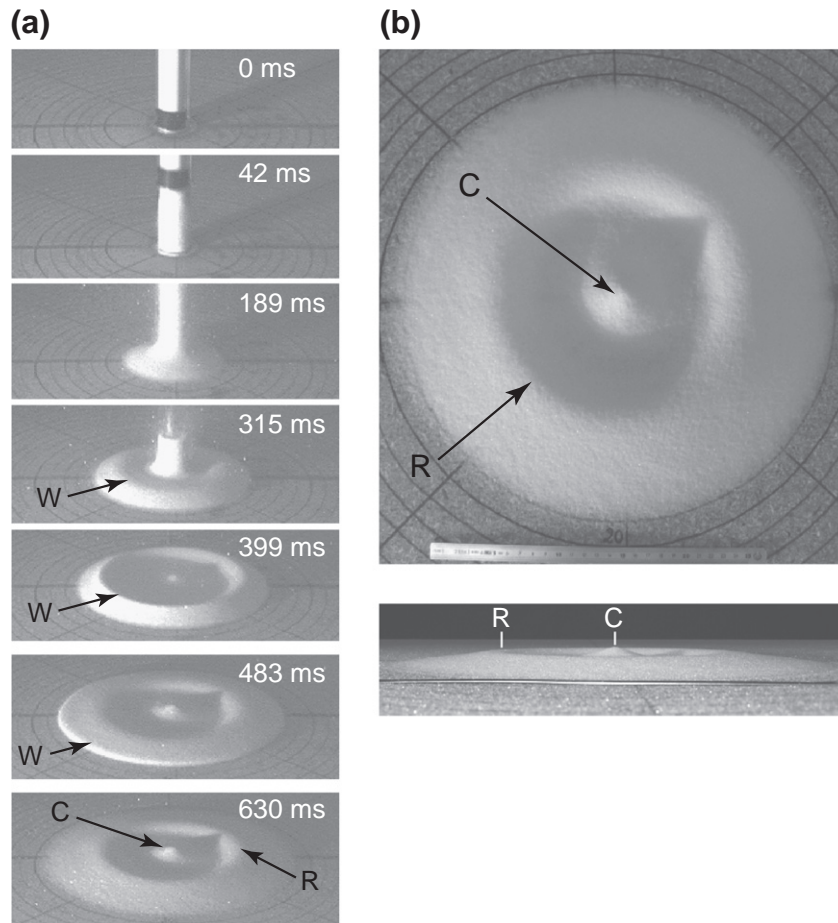


**Fig. 2.** Collapse of a dry column of coarse particles ( $a = 16.7$ ). (a) Snapshots at different times after release. Note the black mark at the base of the uplifted cylinder and circular marks 2 cm apart on the plane. A wave (W) travels at the flow surface, and the final deposit consists of a central cone (C) and of a circular ridge (R) that delimits a depression. As  $a$  increases, the height of the depression decreases and approaches zero at  $a > 18$ –19, whereas that of the ridge increases and becomes close to that of the central cone at  $a > 24$ –25. (b) Top and side view of the deposit.

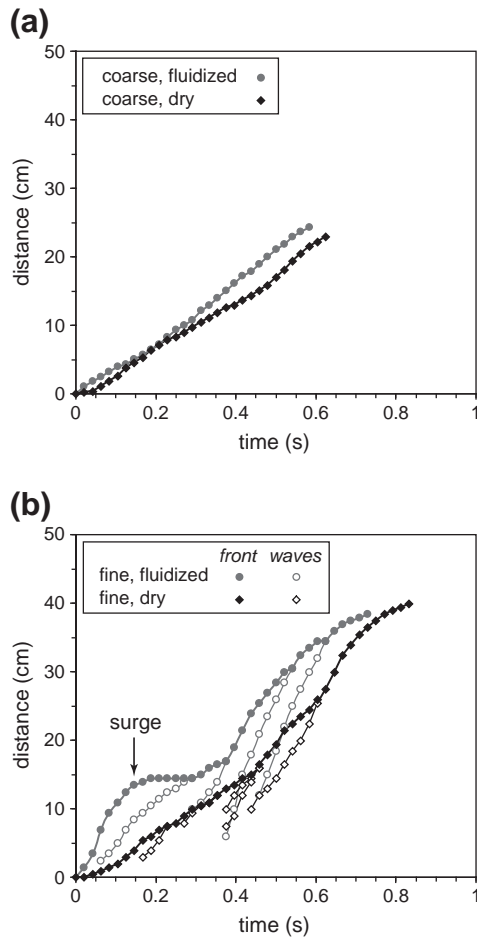


**Fig. 3.** Flow kinematics. Flows of coarse (a) or fine (b) particles generated from dry or fluidized columns at  $a = 26.5$  (with  $r_i = 2.1$  cm). In (a), the position of the surface wave cannot be determined accurately and is not represented. In (b), the position of the initial surge (see Fig. 4c) is indicated, and both the position of the flow front and of the shock waves are represented at the same time. Successive waves are located behind the flow front at a given time and later overtake it to form a new front.

at a higher velocity. Each shock wave propagates at nearly constant velocity, then decelerates and is overtaken by the wave generated after it. In most cases, the wave grows in amplitude, then plunges, brakes, and sometimes splashes. The deposit morphologies are the same as for the coarse particles, but generally with lower transitional aspect ratios (Figs. 1c and 5). However, the surface of the cone and “Mexican-hat” deposits has a ripply structure resulting from late small surface flows, and cone-and-ridge deposits exhibit up to three distinct concentric ridges whose number increases and position is located downstream as  $a$  increases. At very high  $a$  ( $>18$ – $20$ ), the deposits viewed from above are no longer regular disks as their edges are lobate and diffuse (Fig. 5).

Initial fluidization has a strong influence on the column collapse processes, in contrast with the coarse material. It facilitates the formation of the surface waves, as up to 5–6 shock waves form and as the first wave appears at  $a \sim 3$ – $3.5$ , lower than for the initially dry flows (Fig. 4c). In most cases at high  $h_i$  ( $\sim 40$ – $45$  cm), a dilute and thin basal surge spreads radially very rapidly once the cylinder is lifted. The surge then decelerates and stops and, after a while, is overtaken by the first wave (Fig. 3b). As for the initially dry flows of fines, successive shock waves form at increasing distance from the initial column, but, at given initial conditions, appear earlier and commonly last longer. The deposits have morphologies similar to that of the initially dry cases, though the area above the porous plate is horizontal (Fig. 5). They exhibit up to three ridges at  $a > \sim 10$  and their front is lobate for  $a > 14$ – $15$ . Interestingly, at

high  $a$ , the duration and run-out of the initially dry and fluidized flows of fines are very close, as discussed hereafter.

#### 4.2. Scaling laws

The scaling laws of type  $\lambda a^n$  (Eq. (4)) determined in the present study for the normalized flow run-out, deposit height, and position of the ridges, as well as the deposit aspect ratio are reported in Table 1. Not surprisingly, the scaling laws of the normalized flow run-out for the dry coarse material are similar to those determined in earlier studies (Lajeunesse et al., 2004; Lube et al., 2004), though  $r^*$  at given  $a$  is generally slightly larger than reported previously (Fig. 6, see  $\lambda$  values in Tables 1 and S1). Our experiments, however, reveal that when flow friction is reduced through initial fluidization, the scaling laws have the same form as that of these dry flows because  $n = 1$  and  $n = 1/2$  at low and high  $a$ , respectively (except for the initially dry fine particles as discussed hereafter). The run-out increase caused by initial fluidization compared to the dry material is reflected essentially by an increase of the coefficient  $\lambda$ , of only 6–9% for the coarse particles but of 39–77% for the fines. For the fluidized fine particles, transition to the second regime ( $n = 1/2$ ) occurs at  $a \sim 1.1$ , lower than  $a \sim 1.6$  observed for the other cases, and a third regime is identified at  $a > \sim 17$ . For the dry fine particles at  $a > \sim 2$ , the scaling law is different from the other cases because  $n \sim 2/3$ , and we highlight that the data dovetail those of the initially fluidized fine particles at  $a > \sim 4$ .

Our experiments on initially dry fine particles reveal that the scaling laws of the normalized central height of the deposit are similar to that of dry coarse material (Fig. 7). However, the height of the deposit,  $h_f$ , is slightly smaller than  $h_i$  at  $a < \sim 0.7$ , possibly due to compaction related to moderate lateral spreading of the granular pile once released. Note that at  $\sim 1 < a < \sim 10$ ,  $h^*$  for the fine particles is higher than for the coarse ones because of higher values of  $h_f$ , possibly due to moderate ambient moisture and related mild cohesion effects. Nevertheless, corrected  $h_f$  values lead to  $h^*$  values comparable to that of the coarse material (see inset in Fig. 7). Initial fluidization causes decrease of the deposit height, so that  $h^*$  is smaller than in the dry cases. New scaling laws are identified for the coarse particles as  $n = 1/3$  and  $n = -1/2$  at  $a$  below and above  $\sim 5$ , respectively, despite scatter of the data. Note that for the fine particles,  $h^*$  is randomly distributed in the narrow range  $\sim 0.1$ – $0.2$ .

We also report new data on the geometrical characteristics of the deposits. The deposit aspect ratio,  $h_f/r_f$ , decreases from  $O(10^{-1})$  to  $O(10^{-2})$  at increasing  $a$  (Fig. 7). For both the fine and coarse dry materials, scaling laws of type  $h_f/r_f = \beta a^m$  reveal that  $m = 1/2$  and then  $m = -1/2$  as  $a$  increases. When the material is initially fluidized, the deposit aspect ratio is up to one order of magnitude lower than in the dry cases because the central height is much reduced. For the fine particles, the  $h_f/r_f$  data reveal a single trend as  $n = -0.4$ . This contrasts with  $h^* = h_f/r_i$  but can be explained as  $h_f$  actually varies very few and is negligible compared to  $r_f$  that is much larger than  $r_i$ , thus leading to a good trend for the  $h_f/r_f$  data. For the coarse particles,  $n = -0.15$ , and then  $n = -1$  at high  $a$  as for the initially dry fine particles. We also report the normalized position of the ridges,  $(r_r - r_i)/r_i = \gamma a^l$ , in the deposits of fine particles. The data reveal scaling laws with  $l \sim 1/3$ , except for the most inner ridge in case the material is initially dry as  $l \sim 1/2$  (Fig. 8). We acknowledge, however, that the data are scattered.

## 5. Discussion

### 5.1. Characteristics of the experiments

#### 5.1.1. Wave generation process

Our experimental results bring new information on the collapse mechanisms of granular columns and on the characteristics of their resulting deposits. A surface wave forms in initially dry or fluidized flows of coarse (at  $a > 7$ – $8$ ) or fine ( $a > 3$ – $5$ ) particles. This wave develops at aspect ratios at which “Mexican-hat” deposits are well defined

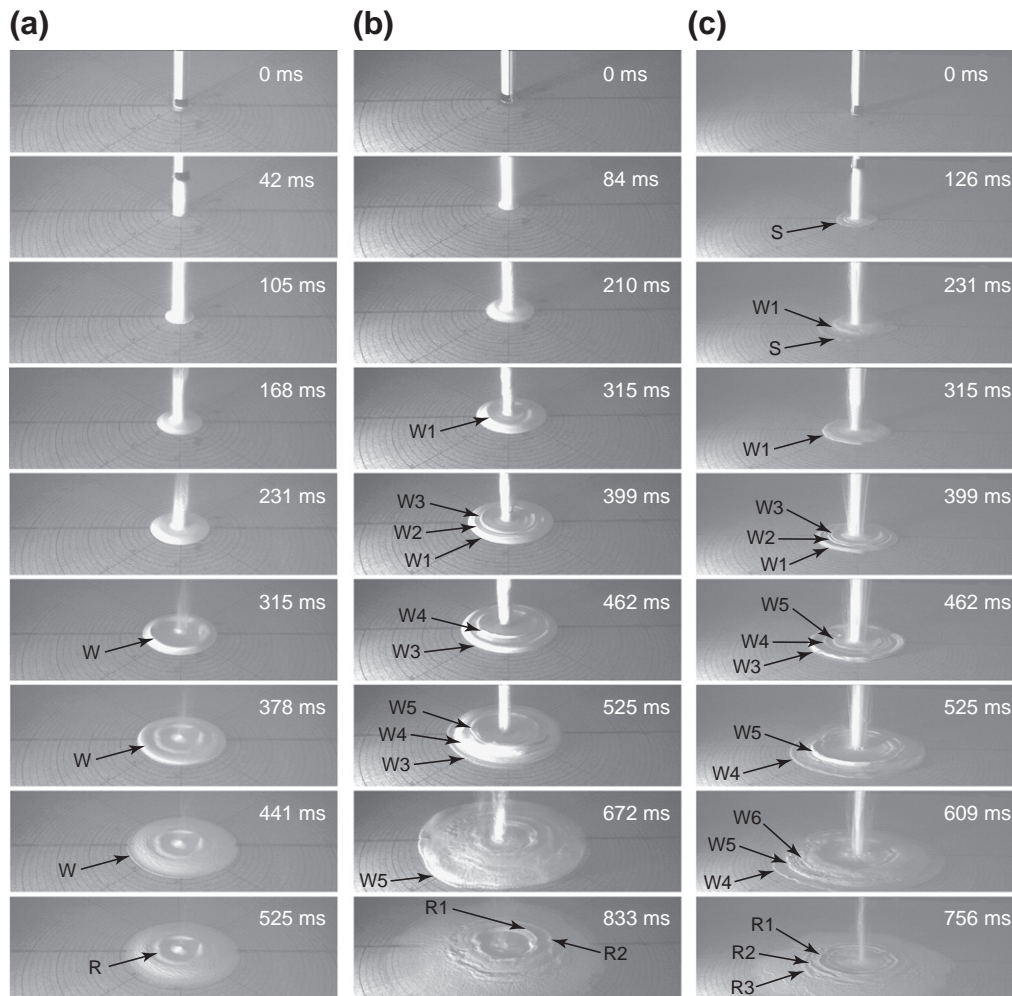


**Fig. 4.** Flow emplacement. Snapshots of the collapse of columns of fine particles, at different times after release. Note the black mark at the base of the uplifted cylinder and circular marks 2 cm apart on the plane. Initial conditions are (a) dry,  $a = 9.6$ ; (b) dry,  $a = 26.4$ ; and (c) fluidized,  $a = 30.4$ , where  $S$  denotes the basal surge.  $W$  and  $R$  indicate surface waves and ridges, respectively, with numbers denoting their order of formation.

and just below those at which cone-and-ridge deposits form. In fact, video analyses confirm that an inflection point or a ridge appears as the rear part of the wave stops abruptly. Note that a similar wave with a related ridge is predicted by discrete and shallow-water numerical simulations of granular column collapse (Larrieu et al., 2006, their Fig. 2; Staron and Hinch, 2005, their Fig. 13; Staron and Hinch, 2007, their Fig. 11) and observed in experiments on granular collapse over inclined beds (Hogg, 2007, his Fig. 6). A more complex configuration is revealed in our experiments at high  $a$  with fine particles as several shock waves and ridges form. The ridges most probably result from the first waves that stop abruptly, as confirmed by their proximal to intermediate position in the deposits. They are then overridden by the last waves that travel the larger distances and do not lead to any distinct morphology at the deposit margin. In flows of initially fluidized fine particles, the early stage surges at high column height most probably result from the rapid release of the basal pressure (proportional to  $h_i$ ) once the cylinder is lifted. Interestingly, these surges resemble the features generated as a vertical granular jet impinges a horizontal solid surface and generates high pressure (Boudet et al., 2007).

#### 5.1.2. Possible auto-fluidization

An important result of our study is that the normalized flow run-out of the initially dry flows of fine particles is equal to that of their initially fluidized counterparts at  $a > 4$  (Fig. 6). This could suggest (partial) auto fluidization of the initially dry flows, which, according to the results described above, would begin to act at  $a \sim 2$  and would

confer at  $a > 4$  a mean degree of fluidization equivalent to that of the initially fluidized flows, hence leading to  $n \sim 2/3$  instead of  $n = 1/2$  due to changing flow dynamics. Recent air pore pressure measurements by Roche et al. (2010) in flows resulting from the collapse of dry columns of the same fine particles (at  $a = 2$ , channel configuration) support the idea of a possible auto fluidization process. These reveal partial support of the weight of the grains and hence partial auto fluidization during flow propagation. Unfortunately, we cannot test our hypothesis on auto fluidization in the present study because the flows are too thin to obtain any treatable signal using the pressure measurement device of Roche et al. (2010). Assuming (partial) auto fluidization occurs, it would not result from the ingestion of the ambient air by the plunging waves as proposed for flows in rotating drums (Bareschino et al., 2008) because these waves form only at  $a > 6-7$ , but rather from shear induced differential air-particle motion (Roche et al., 2008). We acknowledge that the trends for the fine particles could suggest, alternatively, that initial fluidization does not influence the flow behavior at  $a > 4$ . We stress, however, that (1) high pore pressure should be maintained for most the duration of the initially fluidized flows of fines regardless  $a$  (see Section 3), and (2) that the trend of the initially dry flows of fines departs from that of all other types of flows.

#### 5.1.3. Scaling laws of the flow run-out

A key result of our experiments regarding the scaling law  $r^* = \lambda a^n$  in case of initial fluidization is that, compared to the same dry

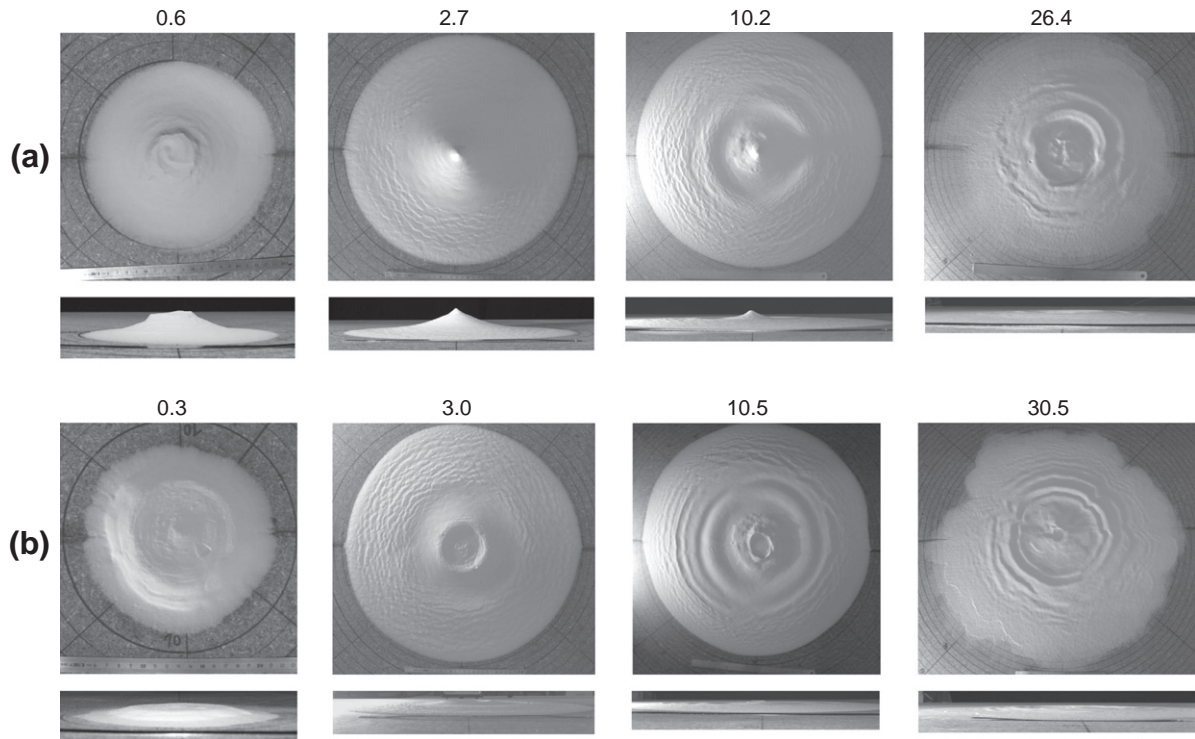


**Fig. 5.** Deposit morphologies. Top and side views of the deposits resulting from collapses of dry (a) or fluidized (b) columns of fine particles. Numbers denote the column aspect ratio,  $a$ . Circular marks on the plane are 2 cm apart. Frontal lobes form at  $a > 18–20$  (dry columns) and  $a > 14–15$  (fluidized columns). In (a), moderate ambient moisture commonly renders the upper slope of the central cone a bit steeper than the angle of repose of the same material but perfectly dry.

material and at given  $a$ , the coefficient  $\lambda$  increases whereas the exponent  $n$  is constant (except for the dry fine particles at high  $a$  whose case is treated in Section 5.1.2). We recall that internal friction is first negligible in the fluidized granular columns and then increases through pore pressure diffusion in the propagating flows. In consequence, the amount of increase of  $\lambda$  reflects a mean friction, lower than that of the dry material and which varies inversely with the pore pressure diffusion timescale, so that the increase in  $\lambda$  is almost negligible for the coarse particles but is significant for the fines. Hence, our study provides experimental evidence of the relevance of Eq. (5) to describe empirically the run-out of fluidized flows. Note that the friction angle  $\delta$  in Eq. (5) is not an intrinsic property of the material, but rather reflects the mean effective friction (i.e., related to the mean energy dissipation) during the flow (see Section 2.2). As predicted by Eq. (5), the reduced granular friction due to fluidization results in an increase of  $\lambda$  (Fig. 6).

Our analysis supports the conclusion of Balmforth and Kerswell (2005) that states that  $\lambda$  is material dependent, which, in light of

our results, can be explained by the relatively large range of material friction angle used in their study (assumed to be equal to the material repose angle  $\phi = 24.5–36.5^\circ$ ). In contrast, this contradicts the findings of Lube et al. (2004) based on experiments involving dry granular materials with friction angles in a very narrow range ( $\phi = 30–35^\circ$ ). Indeed, for this small range of friction angles, numerical simulations show that the effective friction coefficient of the granular medium saturates towards an almost constant value (Mangeny et al., 2006, their Fig. 2). We note that for our initially dry flows at low  $a$ ,  $\lambda$  for the fine material (with  $\phi = 28^\circ$ ) is slightly higher than for the coarse one (with  $\phi = 25^\circ$ ). This does not necessarily contradict the  $\lambda$ -dependence on material properties as (1) both materials may have actually the same friction angle ( $\sim 25^\circ$ ) as the higher repose angle of the fine material could result from moderate ambient moisture effects, and (2) the fine material might experience partial auto fluidization at low  $a$  (see Section 5.1.2), thus causing a higher normalized flow run-out.

Another important result is that the decrease of  $n$  from 1 to 1/2 when  $a$  increases (except for the dry fine particles for which  $n$

**Table 1**  
Scaling laws in the experiments of the present study.

Particle type	Coarse	Coarse	Fine	Fine
Initial condition	Dry	Fluidized	Dry	Fluidized
$r^* = (r_f - r_i)/r_i$ <sup>a</sup>	1.40 $a$ , ( $a < 1.6$ ) 1.82 $a^{1/2}$ , ( $a > 1.6$ )	1.48 $a$ , ( $a < 1.6$ ) 1.99 $a^{1/2}$ , ( $a > 1.6$ )	1.61 $a$ , ( $a < 1.6$ ) 1.84 $a^{-2/3}$ , ( $a > 1.6$ )	2.49 $a$ , ( $a < 1.1$ ) 2.53 $a^{1/2}$ , ( $1.1 < a < 17$ ) 1.68 $a^{0.69}$ , ( $a > 17$ ) <sup>b</sup>
$h^* = h_f/r_i$	$a$ , ( $a < 0.7$ ) $\sim 0.7$ , ( $0.7 < a < 7$ ) <sup>l</sup> $\propto a^{-1/2}$ , ( $a > 7$ ) <sup>l</sup>	0.26 $a^{1/3}$ , ( $a < 5$ ) <sup>c</sup> $a^{-1/2}$ , ( $a > 5$ ) <sup>e</sup>	0.84 $a$ , ( $a < 1$ ) <sup>d</sup> $\sim 0.95$ , ( $1 < a < 6$ ) <sup>l</sup> $\propto a^{-1/2}$ , ( $a > 6$ ) <sup>l</sup>	$\sim 0.1–0.2$
$h_f/r_f$ <sup>g</sup>	0.42 $a^{1/2}$ , ( $a < 0.7$ ) 0.27 $a^{-1/2}$ , ( $a > 0.7$ )	0.10 $a^{-0.15}$ , ( $a < 5$ ) 0.43 $a^{-1}$ , ( $a > 5$ ) <sup>j</sup>	0.29 $a^{1/2}$ , ( $a < 1$ ) <sup>h</sup> 0.33 $a^{-1/2}$ , ( $1 < a < 6$ ) 0.78 $a^{-1}$ , ( $a > 6$ ) $\propto a^{-1/2}$ , (1st ridge) $\propto a^{-1/3}$ , (2nd ridge)	0.05 $a^{-0.4}$ , <sup>i</sup>
$(r_f - r_i)/r_i$ <sup>k</sup>				$\propto a^{-1/3}$

Regression coefficients are <sup>a</sup>  $> 0.98$ , <sup>b</sup> 0.88, <sup>c</sup> 0.96, <sup>d</sup> 0.86, <sup>e</sup> 0.78, <sup>f</sup> 0.76, <sup>g</sup>  $> 0.97$  (except <sup>h-i</sup> 0.91 and <sup>j</sup> 0.93), and <sup>k</sup> 0.66–0.91. <sup>l</sup> Arbitrary fit.

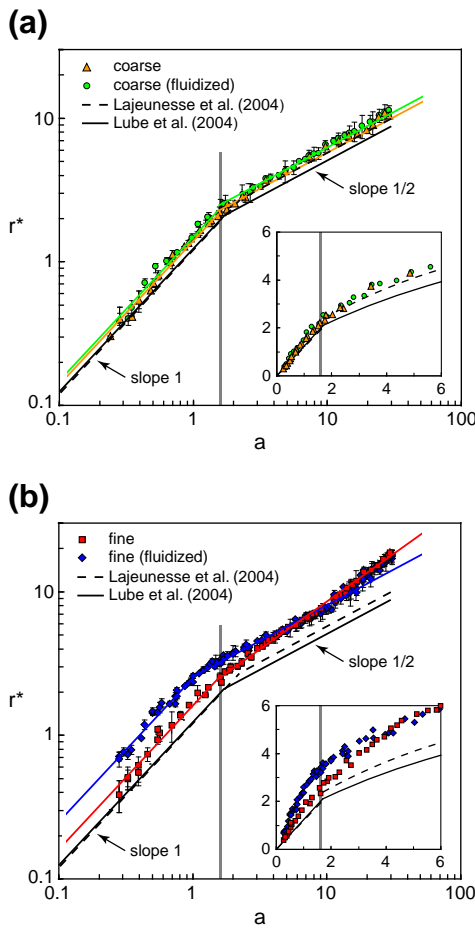


**Fig. 6.** Scaling laws. Normalized flow run-out,  $r^* = (r_f - r_i)/r_i$ , as a function of the column aspect ratio,  $a$ , for the (a) coarse and (b) fine particles. The inserts show the data at low  $a$  with linear scales. The vertical gray bars indicate the aspect ratio ( $\sim 1.6$ ) at which the shift in scaling law occurs for the dry flows.

decreases to  $\sim 2/3$ , as reported in earlier studies on 3D column collapse of dry coarse material, is also a characteristic of initially fluidized flows. The analysis of Lajeunesse et al. (2004) shows that by approximating deposits of dry flows at high  $a$  as cones then  $r_f/r_i$  is proportional to  $a^{1/2}$  if one assumes that  $h_f/r_i$  is constant (see their Eq. (5)). In this context, we stress that  $r^* = (3ar_i/h_f)^{1/2} - 1$  and that  $r_i/h_f$  is constant only at  $a < \sim 10$  in our experiments (Fig. 7). This means that the axisymmetrical spreading of the column may partly contribute to account for the dependence of  $r^*$  on  $a^{1/2}$  at high  $a$ , but there exists at least another control parameter, yet to identify. We highlight that  $n = 1$  at low  $a$  indicates that  $r_f - r_i = \lambda h_i$ , that is, the flow run-out from the edge of the column is proportional to the original column height, which is the relevant typical length scale for normalizing the flow run-out in the granular column collapse configuration (Lucas and Mangeney, 2007; Roche et al., 2008).

5.2. Comparison with natural data and implications

We now follow the approach of Lucas and Mangeney (2007) and compare our experimental results with data on natural granular mass flows in order to infer their effective friction angle in the context of the thin layer approach and discuss their emplacement mechanisms. We consider the Valles Marineris (VM) landslides on Mars whose emplacement mechanisms are controversial. The data are from Lajeunesse et al. (2006) based on the study of Quantin et al. (2004) after the altimetric MOLA grid (MEGDR products) and the satellite images IR-THEMIS, and independently from Lucas et al. (2011)

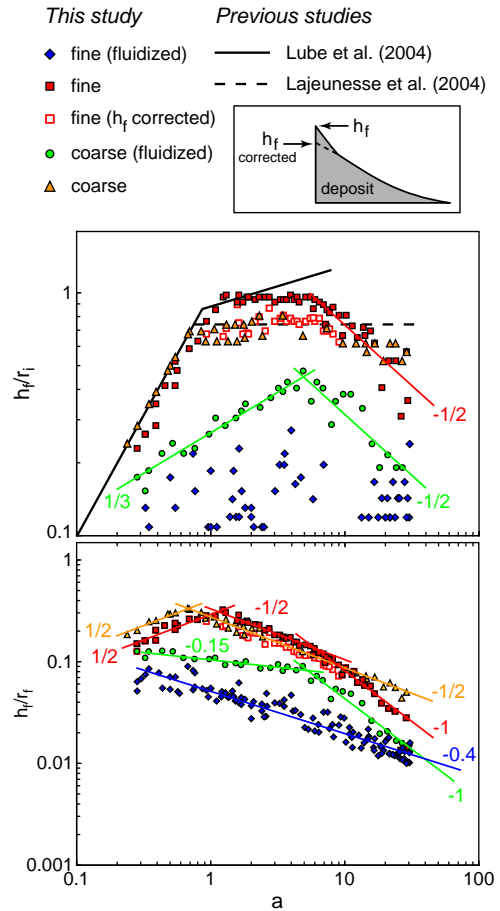


**Fig. 7.** Scaling laws. Normalized central height of the deposits,  $h_f/r_i (= h^*)$  and  $h_f/r_f$  (deposit aspect ratio), as a function of the column aspect ratio,  $a$ . The sketch in inset represents a half deposit of fine particles with the actual central height ( $h_f$ ). In the case of dry fine particles, corrected values of the height are considered by assuming a constant upper slope of the deposit (dashed line in inset, see text for details).

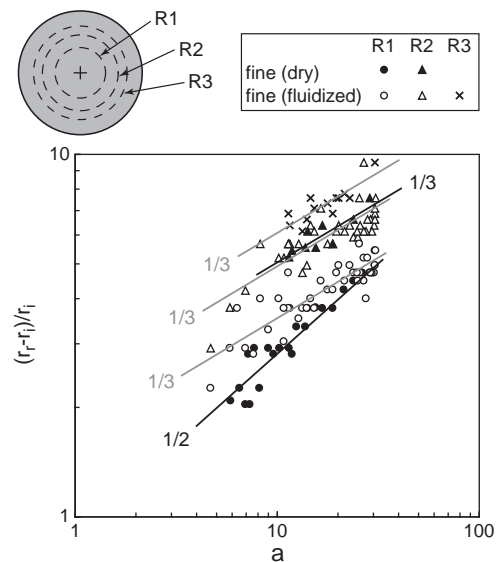


**Fig. 8.** Scaling laws. Normalized position of the ridges,  $(r_f - r_i)/r_i$ , in deposits of fine particles as a function of the column aspect ratio,  $a$ . The sketch represents a deposit viewed from above, with the relative position of the ridges ( $R$ ). Actual fits indicate a slope of 0.52 ( $n \sim 1/2$ ) with a regression coefficient of 0.91 for the inner ridge ( $R_1$ ) of the dry flow deposits and of 0.32–0.34 ( $n \sim 1/3$ ) with regression coefficients of 0.66–0.77 in all other cases.

after CTX and HRSC images in addition to MOLA shots (PEDR products) and THEMIS data sets. The run-out data of Lajeunesse et al. (2006) define a scaling law similar to that in experiments on dry granular flows (i.e.,  $n \sim 1$ ). Recent complementary data of Lucas et al. (2011), however, show that the trend is not as clear (see Fig. 9). Nevertheless, these landslides provide a unique data set for comparison with laboratory experiments and thin layer approaches for the following reasons. (1) They derive from the collapse of steep cliffs and lay on a nearly flat substrate ( $1\text{--}2^\circ$ ), so that the granular column collapse configuration is a good analog of these events. Note that the shape of the released masses is not exactly a column but this almost does not affect the run-out distance, even though the detail of the deposit morphology can be sensitive (Lucas et al., in 2011; Thompson and Huppert, 2007). (2) The aspect ratio of the mobilized material is small ( $a < 1$ ). (3) The geometrical parameters of the released masses (i.e.,  $r_i$  and  $h_i$ ) and of their resulting deposits (i.e.,  $r_f$  and  $h_f$ ) can be well constrained thanks to the absence of vegetation and a very low erosion rate since the landslides emplacement. This contrasts fundamentally with terrestrial cases and explains why data for a range of  $a$  are not available in literature. As pointed out by Lucas and Mangeney (2007), based on the analysis of Mangeney-Castelnau et al. (2005), though gravity acceleration on Mars is smaller than on Earth and density (and to some extent size) of the particles may be different from that in experiments, these parameters only affect the dynamic variables so that only the flow velocity and the duration of emplacement are gravity dependent (cf. Meruane et al., 2010). This is true if the friction coefficient is not gravity dependent, and in this context we stress that a variable coefficient (e.g., Pouliquen and Forterre, 2002) would not allow to reproduce the experimental scaling laws (see Section 3.2 of Mangeney-Castelnau et al., 2005).

Fig. 9 shows that the normalized run-out of the VM landslides is higher at given  $a$  than that of our experimental flows, including those with low friction. This result can be interpreted in two ways: either (1) the physical mechanisms that control the emplacement of the granular masses are length scale dependent (i.e., the forces are of different relative

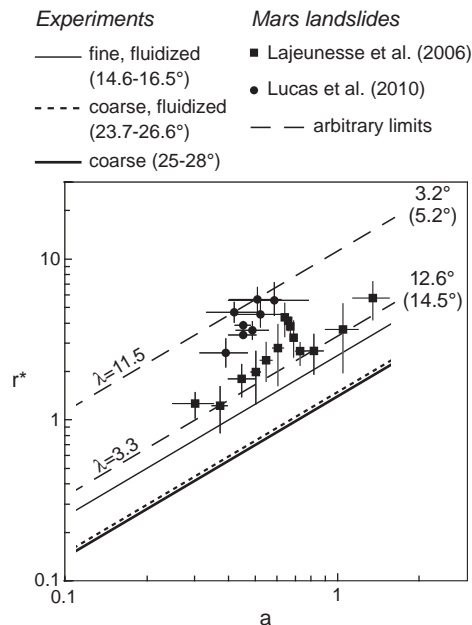


**Fig. 9.** Comparison with natural cases. Normalized run-out distance of the Valles Marineris (Mars) landslides (Lajeunesse et al., 2006; Lucas et al., 2011) and of our experimental flows as a function of the aspect ratio,  $a$ . Note that Lucas et al. (2011) consider landslides whose propagation was not constrained by any topographic barrier. Effective friction angles in the context of the thin layer approach are indicated. Low angles are inferred for the VM landslides, whose data are delimited by large dashed lines corresponding to  $\lambda \sim 3.3$  and  $\lambda \sim 11.5$ , assuming no regional slope or a slope of  $2^\circ$ , respectively (numbers in bracket).

magnitude at the laboratory and natural scale), or (2) assuming scale independence, the mean energy dissipation of the VM landslides (i.e. the mean effective friction coefficient) is lower than that of a frictional dry granular material as proposed by Lucas and Mangeney (2007). The following discussion deals with the second hypothesis. The study of Lucas and Mangeney (2007) shows from numerical modeling on real 3D topography that though the gentle regional slope (up to  $\sim 2^\circ$ ) at Valles Marineris can explain a run-out increase it is not high enough to account for the natural data if one assumes energy dissipation equivalent to that of a frictional dry granular material. In light of our experimental results, the contribution of at least one mechanism proposed in the literature to explain low energy dissipation in natural granular flows (see Section 1) should be considered. In particular, friction reduction due to the presence of a fluid as proposed by Luchitta (1979), McKenzie et al. (2002), and Quantin et al. (2004) cannot be ruled out for the VM landslides (though some other mechanisms might have operated), in contrast to the findings of McEwen (1989) and Lajeunesse et al. (2006).

Eq. (5) provides estimates of the effective friction angles from  $\lambda$  values. First, we take into account  $\lambda$  values for the VM landslides ( $\sim 3.3 < \lambda < \sim 11.5$ , from Fig. 9) and for our experiments at  $a < 1.6$  ( $n = 1$ , Table 1). Considering our dry coarse granular flows and assuming  $\delta = 25\text{--}28^\circ$  (cf. Mangeney-Castelnau et al., 2005), we obtain  $\alpha = 0.65\text{--}0.74$ . With these values of  $\alpha$ , we deduce  $\delta = 14.6\text{--}16.5^\circ$  and  $\delta = 23.7\text{--}26.6^\circ$  for our initially fluidized flows of fine and coarse materials, respectively, whereas  $\delta = 3.2\text{--}12.6^\circ$  (no regional slope) and  $\delta = 5.2\text{--}14.5^\circ$  ( $\theta = 2^\circ$ ) for the VM landslides (Fig. 9). Note that these last values of  $\delta$  encompass those needed in numerical simulations of flows over realistic 3D topography to fit the natural deposits (Lucas and Mangeney, 2007; Lucas et al., 2011). Low energy dissipation in the VM landslides is confirmed as well by discrete element models. The study of Smart et al. (2010) shows that internal and basal friction angles as small as  $5.7^\circ$  and  $0^\circ$ , respectively, for half the travel distance are required to simulate the large run-out of these landslides. Even if small energy dissipation is not mentioned explicitly in Staron (2008), their discrete element models also require friction angles between the grains lower than  $\delta = 5^\circ$  to account for the landslides run-out distances (see their Fig. 8), even though the simulations are performed on steeper slopes. The same simulations using a friction angle  $\delta = 45^\circ$  overestimate by a factor  $\sim 2$  the run-out distance of experimental granular flows (i.e.,  $\lambda = 2.5$  instead of 1.2; Staron and Hinch, 2005, their Fig. 6). The work of Lacaze et al. (2008) suggests that DEM simulations only reproduce quantitatively experimental results with appropriate friction angles when the experimental setup is correctly simulated (i.e., 2D planar experiments have to be simulated using 3D configurations taking into account wall friction).

## 6. Conclusion

Our experimental investigation on the emplacement of geophysical granular flows complements earlier works on dry granular materials as it addresses flows of lower friction resulting from the collapse of fluidized columns. Internal friction is negligible in the initial columns and then increases in the propagating flows as pore pressure diffuses. Hence, initial fluidization has little influence on flows of coarse ( $d \sim 330 \mu\text{m}$ ) particles because pore pressure diffuses rapidly and internal friction is reacquired almost instantaneously. In contrast, high pore pressure is maintained for most the duration of the flows of fine ( $d \sim 75 \mu\text{m}$ ) particles, thus conferring a low mean friction.

The modes of flow propagation and the scaling laws that characterize the morphology of the deposits provide information on the flow dynamics. Waves are present at the surface of the flows at high aspect ratios ( $a > \sim 3\text{--}7$ ) and in many cases lead to the formation of ridges in the deposits, suggesting that such structures could exist in nature in case of similar initial conditions. The normalized flow run-out is equal to  $\lambda a^n$ , as shown in previous studies on dry flows of coarse grains. Our results reveal, however, (1) that the coefficient  $\lambda$

varies inversely with the mean friction of the flow, thus providing experimental evidence of the relevance of the analytical law of Lucas and Mangeney (2007, Eq. 5), and (2) that the exponent  $n$  is independent of that mean friction. More importantly, our results show that these scaling laws are not only typical of dry granular flows, as claimed in the literature, but also characterize flows of low friction and thus low energy dissipation. The decrease of  $n$  from 1 to 1/2 at increasing  $a$  (except for the dry fine material) reflects mainly axisymmetrical spreading of the granular column (i.e., Lajeunesse et al., 2004). In this context, we highlight that values of  $n < 1$  at high  $a$  in experiments on dry flows in the channel configuration may reflect essentially sides effects, which is supported by the fact that  $n$  approaches one when the channel width increases (e.g., Balmforth and Kerswell, 2005, see Table S1). This suggests that when axisymmetrical spreading is negligible (i.e.,  $n = 1$  and  $r_f - r_i = \lambda h_i$ ), in 2D or at low  $a$  in 3D, the flow run-out from the edge of the column that results from a conversion of potential energy into kinetic energy is simply proportional to the original column height, which is the relevant length scale parameter, and varies inversely with the mean energy dissipation (Lucas and Mangeney, 2007; Roche et al., 2008). Note, however, that the initial width,  $r_i$ , used in earlier investigations to normalize the flow run-out is useful to obtain elegant data collapse and well-defined scaling laws for the column collapse configuration (Lajeunesse et al., 2004; Lube et al., 2004).

Our study reveals that initially dry flows of fine particles could experience (partial) auto fluidization (cf. Roche et al., 2010). In this context, the exponent  $n \sim 2/3$  at high  $a$  may result from the combination of this effect and of axisymmetrical spreading (cf.  $n = 1/2$ ). Auto-fluidization is appealing to account for the long run-out distance of dense gas–particle mixtures such as pyroclastic flows, and this will be addressed in detail in future investigations.

Comparison of our experimental results with published data on the Valles Marineris (VM) landslides on Mars shows, if one assumes that the physical processes are length-scale independent, that energy dissipation for these natural flows is much lower than that of typical dry frictional granular materials, in agreement with Lucas and Mangeney (2007) and Lucas et al. (2011). Following Lucas and Mangeney (2007) in the context of the thin layer approach we determine effective friction angles  $\sim 15^\circ$  for the VM landslides, thus suggesting that a least one physical mechanism contributed to low energy dissipation during their emplacement. The method applied to treat the VM landslides data can be used as well for any type of terrestrial granular flows for which the column collapse configuration is relevant.

## Acknowledgments

Eric Lajeunesse communicated his data on Valles Marineris landslides. This work was supported by the Institut de Recherche pour le Développement (IRD, France), and the ANR Volbiflo and Planeteros projects (France). The paper benefited from useful comments of three anonymous reviewers.

## Appendix A. Supplementary data

Supplementary data to this article can be found online at doi:10.1016/j.epsl.2011.09.023.

## References

- Balmforth, N.J., Kerswell, R.R., 2005. Granular collapse in two dimensions. *J. Fluid Mech.* 538, 399–428. doi:10.1017/S0022112005005537.
- Bareschino, P., Lirer, L., Marzocchella, A., Petrosino, P., Salatino, P., 2008. Self-fluidization of subaerial rapid granular flows. *Powder Technol.* 182, 323–333. doi:10.1016/j.powtec.2007.12.010.
- Boudet, J.-F., Amarouchene, Y., Bonnier, B., Kellay, H., 2007. The granular jump. *J. Fluid Mech.* 572, 413–431. doi:10.1017/S002211200600365X.
- Collins, G.S., Melosh, H.J., 2003. Acoustic fluidization and the extraordinary mobility of sturzstroms. *J. Geophys. Res.* 108, 2473. doi:10.1029/2003JB002465.
- De Blasio, F.V., Elverhøi, A., 2008. A model for frictional melt production beneath large rock avalanches. *J. Geophys. Res.* 113, F02014. doi:10.1029/2007JF000867.
- Geldart, D., 1986. *Gas Fluidization Technology*. Wiley and Sons Ltd.
- Girolami, L., Druitt, T.H., Roche, O., Khrabrykh, Z., 2008. Propagation and hindered settling of laboratory ash flows. *J. Geophys. Res.* 113, B02202. doi:10.1029/2007JB005074.
- Girolami, L., Roche, O., Druitt, T.H., Corpetti, T., 2010. Velocity fields and depositional processes in laboratory ash flows. *Bull. Volcanol.* 72, 747–759. doi:10.1007/s00445-010-0356-9.
- Goren, L., Aharonov, E., 2007. Long runout landslides: the role of frictional heating and hydraulic diffusivity. *Geophys. Res. Lett.* 34, L07301. doi:10.1029/2009GL028895.
- Hayashi, J.N., Self, S., 1992. A comparison of pyroclastic flow and debris avalanche mobility. *J. Geophys. Res.* 97, 9063–9071.
- Hogg, A.J., 2007. Two-dimensional granular slumps down slopes. *Phys. Fluids* 19, 093301.
- Hungr, O., Evans, S.G., 2004. Entrainment of debris in rock avalanches: an analysis of a long run-out mechanism. *Geol. Soc. Am. Bull.* 116, 1240–1252.
- Iverson, R.M., Denlinger, R.P., 2001. Flow of variably fluidized granular masses across three-dimensional terrain 1. Coulomb mixture theory. *J. Geophys. Res.* 106, 537–552.
- Iverson, R.M., Reid, M.E., Logan, M., LaHusen, R.G., Godt, J.W., Griswold, J.P., 2011. Positive feedback and momentum growth during debris-flow entrainment of wet bed sediment. *Nat. Geosci.* 4, 116–121. doi:10.1038/NNGEO1040.
- Kerswell, R.R., 2005. Dam break with Coulomb friction: a model for granular slumping? *Phys. Fluids* 17, 057101. doi:10.1063/1.1870592.
- Kuo, C.Y., Tai, Y.C., Bouchut, F., Mangeney, A., Pelanti, M., Chen, R.F., Chang, K.J., 2009. Simulation of Tsaoling Landslide, Taiwan, based on Saint Venant equations over general topography. *Eng. Geol.* 104 (3–4), 181–189.
- Lacaze, L., Phillips, J.C., Kerswell, R.R., 2008. Planar collapse of a granular column: experiments and discrete element simulations. *Phys. Fluids* 20, 063302. doi:10.1063/1.2929375.
- Lajeunesse, E., Mangeney-Castelnau, A., Vilotte, J.-P., 2004. Spreading of a granular mass on a horizontal plane. *Phys. Fluids* 16, 2371–2381. doi:10.1063/1.1736611.
- Lajeunesse, E., Monnier, J.B., Homsy, G.M., 2005. Granular slumping on a horizontal surface. *Phys. Fluids* 17, 103302. doi:10.1063/1.2087687.
- Lajeunesse, E., Quantin, C., Allemand, P., Delacourt, C., 2006. New insights on the runout of large landslides in the Valles Marineris canyons, Mars. *Geophys. Res. Lett.* 33, L04403. doi:10.1029/2005GL025168.
- Larrieu, E., Staron, L., Hinch, E.J., 2006. Raining into shallow water as a description of the collapse of a column of grains. *J. Fluid Mech.* 554, 259–270. doi:10.1017/S0022112005007974.
- Legros, F., 2002. The mobility of long run-out landslides. *Eng. Geol.* 63, 301–331.
- Linares-Guerrero, E., Goujon, C., Zenit, R., 2007. Increased mobility of bidisperse granular avalanches. *J. Fluid Mech.* 593, 475–504. doi:10.1017/S0022112007008932.
- Lube, G., Huppert, H.E., Sparks, R.S.J., Hallworth, M.A., 2004. Axisymmetric collapses of granular columns. *J. Fluid Mech.* 508, 175–199. doi:10.1017/S0022112004009036.
- Lube, G., Huppert, H.E., Sparks, R.S.J., Freundt, A., 2005. Collapses of two-dimensional granular columns. *Phys. Rev. E* 72, 041301. doi:10.1103/PhysRevE.72.041301.
- Lucas, A., Mangeney, A., 2007. Mobility and topographic effects for large Valles Marineris landslides on Mars. *Geophys. Res. Lett.* 34, L10201. doi:10.1029/2007GL029835.
- Lucas, A., Mangeney, A., Mège, D., Bouchut, F., 2011. Influence of the scar geometry on landslide dynamics and deposits: application to Martian landslides. *J. Geophys. Res.* doi:10.1029/2011JE003803.
- Luchitta, B., 1979. Landslides in Valles Marineris, Mars. *J. Geophys. Res.* 84, 8097–8113.
- Mangeney, A., 2011. Geomorphology: landslide boost from entrainment. *Nat. Geosci.* 4, 77–78.
- Mangeney, A., Heinrich, P., Roche, R., 2000. Analytical and numerical solution of the dam-break problem for application to water floods, debris and dense snow avalanches. *Pure Appl. Geophys.* 157, 1081–1096.
- Mangeney, A., Staron, L., Volfson, D., Tsimring, L., 2006. Comparison between discrete and continuum modeling of granular spreading. *WSEAS Trans. Math.* 2, 373–380.
- Mangeney, A., Tsimring, L.S., Volfson, D., Aranson, I.S., Bouchut, F., 2007. Avalanche mobility induced by the presence of an erodible bed and associated entrainment. *Geophys. Res. Lett.* 34, L22401.
- Mangeney, A., Roche, O., Hungr, O., Mangold, N., Faccanoni, G., Lucas, A., 2010. Erosion and mobility in granular collapse over sloping beds. *J. Geophys. Res.* 115, F03040. doi:10.1029/2009JF001462.
- Mangeney-Castelnau, A., Bouchut, F., Vilotte, J.-P., Lajeunesse, E., Aubertin, A., Pirulli, M., 2005. On the use of Saint-Venant equations for simulating the spreading of a granular mass. *J. Geophys. Res.* 110, B09103. doi:10.1029/2004JB003161.
- McEwen, A.S., 1989. Mobility of large rock avalanches: evidence from Valles Marineris, Mars. *Geology* 17, 1111–1114.
- McKenzie, D., Barnett, D.N., Yuan, D.-N., 2002. The relationship between Martian gravity and topography. *Earth Planet. Sci. Lett.* 195, 1–16.
- Mériaux, C., 2006. Two dimensional fall of granular columns controlled by slow horizontal withdrawal of a retaining wall. *Phys. Fluids* 18, 093301. doi:10.1063/1.2335477.
- Meruane, C., Tamburrino, A., Roche, O., 2010. On the role of the ambient fluid on gravitational granular flow dynamics. *J. Fluid Mech.* 648, 381–404. doi:10.1017/S0022112009993181.
- Montserrat, S., Tamburrino, A., Niño, Y., Roche, O., 2007. Kinematics and pore pressure dynamics in aerated granular flows. *Proc. 32nd Int. Assoc. Hydraulic Res. Congress.*
- Phillips, J.C., Hogg, A.J., Kerswell, R.R., Thomas, N.H., 2006. Enhanced mobility of granular mixtures of fine and coarse particles. *Earth Planet. Sci. Lett.* 246, 466–480. doi:10.1016/j.epsl.2006.04.007.

- Pirulli, M., Mangeney, A., 2008. Result of back-analysis of the propagation of rock avalanches as a function of the assumed rheology. *Rock Mech. Rock Eng.* 41, 59–84.
- Pouliquen, O., Forterre, Y., 2002. Friction law for dense granular flows: application to the motion of a mass down a rough inclined plane. *J. Fluid Mech.* 453, 133–151. doi:10.1017/S0022112001006796.
- Quantin, C., Allemand, P., Delacourt, C., 2004. Morphology and geometry of Valles Marineris landslides. *Planet. Space Sci.* 52, 1011–1022. doi:10.1016/j.pss.2004.07.016.
- Roche, O., Gilbertson, M.A., Phillips, J.C., Sparks, R.S.J., 2002. Experiments on deaerating granular flows and implications for pyroclastic flow mobility. *Geophys. Res. Lett.* 29, 40. doi:10.1029/2002GL014819.
- Roche, O., Gilbertson, M.A., Phillips, J.C., Sparks, R.S.J., 2005. Inviscid behaviour of fines-rich pyroclastic flows inferred from experiments on gas-particle mixtures. *Earth Planet. Sci. Lett.* 240, 401–414. doi:10.1016/j.epsl.2005.09.053.
- Roche, O., Montserrat, S., Niño, Y., Tamburrino, A., 2008. Experimental observations of water-like behavior of initially fluidized, dam break granular flows and their relevance for the propagation of ash-rich pyroclastic flows. *J. Geophys. Res.* 113, B12203. doi:10.1029/2008JB005664.
- Roche, O., Montserrat, S., Niño, Y., Tamburrino, A., 2010. Pore fluid pressure and internal kinematics of gravitational laboratory air-particle flows: insights into the emplacement dynamics of pyroclastic flows. *J. Geophys. Res.* 115, B09206. doi:10.1029/2009JB007133.
- Shreve, R.L., 1968. Leakage and fluidization in air-layer lubricated avalanches. *Geol. Soc. Am. Bull.* 79, 653–658.
- Smart, K.J., Hooper, D.M., Sims, D.W., 2010. Discrete element modeling of landslides in Valles Marineris, Mars. 2010 Fall Meeting, AGU, San Francisco, abstract P51B-1430.
- Staron, L., 2008. Mobility of long-runout rock flows: a discrete numerical investigation. *Geophys. J. Int.* 172, 455–463. doi:10.1111/j.1365-246X.2007.03631.x.
- Staron, L., Hinch, E.J., 2005. Study of the collapse of granular columns using two-dimensional discrete-grain simulation. *J. Fluid Mech.* 545, 1–27. doi:10.1017/S0022112005006415.
- Staron, L., Hinch, E.J., 2007. The spreading of a granular mass: role of grain properties and initial conditions. *Granular Matter* 9, 205–217. doi:10.1007/s10035-006-0033-z.
- Staron, L., Lajeunesse, E., 2009. Understanding how volume affects the mobility of dry debris flows. *Geophys. Res. Lett.* 36, L12402. doi:10.1029/2009GL038229.
- Thompson, E.L., Huppert, H.E., 2007. Granular column collapses: further experimental results. *J. Fluid Mech.* 575, 177–186. doi:10.1017/S0022112006004563.
- Zenit, R., 2005. Computer simulations of the collapse of a granular column. *Phys. Fluids* 17, 031703. doi:10.1063/1.1862240.